How Do Azoles Inhibit Cytochrome P450 Enzymes? A Density Functional Study†

Philip R. Balding,[‡,§] Cristina S. Porro,[‡,§] Kirsty J. McLean,[‡,¶] Michael J. Sutcliffe,[‡,§] Jean-Didier Maréchal,[‡,§,||] Andrew W. Munro,*[,‡,¶] and Sam P. de Visser*[,‡,§]

Manchester Interdisciplinary Biocentre, School of Chemical Engineering and Analytical Science, and Faculty of Life Sciences, The University of Manchester, 131 Princess Street, Manchester M1 7DN, United Kingdom

Received: March 10, 2008; Revised Manuscript Received: April 3, 2008

To examine how azole inhibitors interact with the heme active site of the cytochrome P450 enzymes, we have performed a series of density functional theory studies on azole binding. These are the first density functional studies on azole interactions with a heme center and give fundamental insight into how azoles inhibit the catalytic function of P450 enzymes. Since azoles come in many varieties, we tested three typical azole motifs representing a broad range of azole and azole-type inhibitors: methylimidazolate, methyltriazolate, and pyridine. These structural motifs represent typical azoles, such as econazole, fluconazole, and metyrapone. The calculations show that azole binding is a stepwise mechanism whereby first the water molecule from the resting state of P450 is released from the sixth binding site of the heme to create a pentacoordinated active site followed by coordination of the azole nitrogen to the heme iron. This process leads to the breaking of a hydrogen bond between the resting state water molecule and the approaching inhibitor molecule. Although, formally, the water molecule is released in the first step of the reaction mechanism and a pentacoordinated heme is created, this does not lead to an observed spin state crossing. Thus, we show that release of a water molecule from the resting state of P450 enzymes to create a pentacoordinated heme will lead to a doublet to quartet spin state crossing at an $Fe-OH_2$ distance of approximately 3.0 Å, while the azole substitution process takes place at shorter distances. Azoles bind heme with significantly stronger binding energies than a water molecule, so that these inhibitors block the catalytic cycle of the enzyme and prevent oxygen binding and the catalysis of substrate oxidation. Perturbations within the active site (e.g., a polarized environment) have little effect on the relative energies of azole binding. Studies with an extra hydrogen-bonded ethanol molecule in the model, mimicking the active site of the CYP121 P450, show that the resting state and azole binding structures are close in energy, which may lead to chemical equilibrium between the two structures, as indeed observed with recent protein structural studies that have demonstrated two distinct azole binding mechanisms to P450 heme.

Introduction

The cytochromes P450 (P450s) are a ubiquitous family of enzymes found in a very broad range of organisms, from bacteria and fungi through to plants and mammals.[1] They catalyze a large variety of reactions, of which the most common are oxidations and hydroxylations. Other P450 reactions including reduction, desaturation, ester cleavage, ring expansion, dehydration, and one-electron oxidation have also been reported.[2] P450s in nature have a large number of important biochemical functions. A key role is protection, for example, in the metabolism of xenobiotics.[3] A major example of this in humans is the enzyme CYP3A4, which is the most abundant P450 in the human body and contributes to the metabolism of around half of all drugs in use today.[4] Another role of P450s is in the biosynthesis of important biomolecules, for use as, for example, signal molecules in control of development and homeostasis and regulation of physiological processes.[5] P450s are important drug targets in fungal infections[6] and are, for example, responsible for insecticide resistance in the mosquito.[7] Furthermore, multiple P450s are present in the genome of *Mycobacterium tuberculosis*, the pathogenic bacterium responsible for the disease tuberculosis.[8] In this particular case, azole- and triazole-based P450 inhibitors were shown to coordinate tightly to P450 enzymes from the bacterium (including CYP121 and CYP51B1) and to inhibit mycobacterial growth.[9,10]

Many drug-metabolizing P450s are located in the liver and can inadvertently be inhibited by treatments given to the patient for specific medical conditions. Alternatively, P450-mediated oxidation of certain drugs can alter their biological activity and subsequently lead to potentially harmful drug−drug interactions.[11] Due to this, several prominent drugs have been withdrawn from the market, such as clozapine and fluoxetine, as well as triazolam and amitriptyline.[12] There are several reversible inhibitors with azole functional groups that target the P450s. One of the first P450 inhibitors to be widely employed was metyrapone, which targeted the 11β-hydroxylase P450 (CYP11B1) in the treatment of Cushing's syndrome.[13] Scheme 1 shows chemical structures of metyrapone, fluconazole, and econazole, all of which are regarded as azole inhibitors. Metyrapone has a pyridine functional group, rather than an imidazole or triazole, but due to structural and functional similarities to the azole class, we will include these types of inhibitors here. Fluconazole is a systemically tolerated azole

† Part of the "Sason S. Shaik Festschrift".

* To whom correspondence should be addressed. E-mail: sam.devisser@manchester.ac.uk (S.P.V.); andrew.munro@manchester.ac.uk (A.W.M.).

‡ Manchester Interdisciplinary Biocentre.

§ School of Chemical Engineering and Analytical Science.

¶ Faculty of Life Sciences.

|| Present address: Chemistry Department, University Autonomous of Barcelona, 08193 Bellaterra, Catalonia, Spain.

10.1021/jp802087w CCC: $40.75
Published on Web 06/18/2008

SCHEME 1: Examples of Three Typical Azole Inhibitors of P450 Enzymes, As Studied in This Work

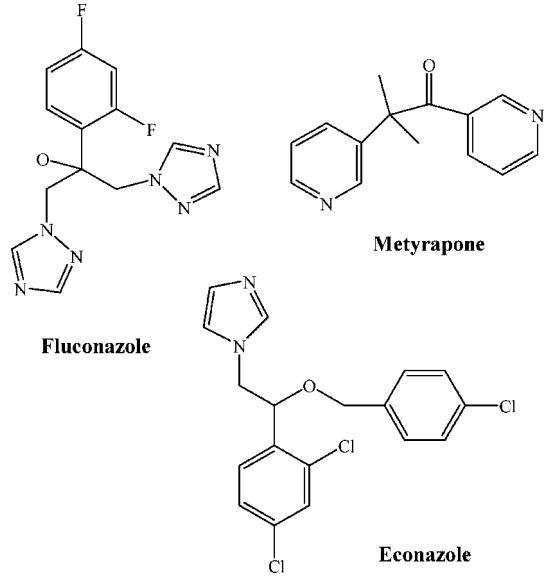

widely used to inhibit the sterol demethylase CYP51 and to treat *Candidiasis*,[14] while econazole is a topical treatment for yeast and fungal infections and was recently shown to be effective in clearing *M. tuberculosis* from infected mice.[15]

The binding of azole drugs to P450s has been extensively studied. As early as 1967, Estabrook et al.[16] reported type-II spectral shifts arising from the binding of nitrogen-containing compounds, such as pyridine and nicotine, to human liver P450s. Van den Bossche postulated that the target of the azole antifungal drugs was the P450 sterol 14α-demethylase, later to be called CYP51.[17] Schuster studied the effect of azoles on human P450s, concluding that the metabolism of xenobiotic substrates would be impeded by azole drugs.[18] Since then, there have been innumerable reports of the binding of azole antifungals to P450s, including many studies on drug−drug interactions involving azole binding to CYP3A4[19] and a number of studies of the binding of azole antifungals to *Mycobacterium tuberculosis* (Mtb) P450s.[20] The first crystal structures of azole-bound P450s were for the fluconazole and phenylimidazole complexes of Mtb CYP51B1, and these showed a nitrogen atom of fluconazole or 4-phenylimidazole coordinated to the heme iron.[21] The inhibitor binds directly to the iron and forms an Fe−N bond. The bulky fluconazole induced structural changes in the active site and in putative ligand entry/exit regions of the P450. Crystal structures have also been solved for the ketoconazole complex with *Saccharopolyspora erythraea* $P450_{eryF}$, for the *Pseudomonas putida* camphor hydroxylase $P450_{cam}$ in complex with imidazole, and for human CYP3A4 bound to ketoconazole.[22] Recently, a high-resolution crystal structure was solved for the *M. tuberculosis* CYP121 bound to fluconazole.[23] Nitric oxide synthase, an oxidase enzyme with heme coordination similar to that of the P450s, is also inhibited by imidazole, which binds to form a low-spin complex.[24,25]

The active center of P450 enzymes contains a central heme moiety that is linked to the protein backbone via an Fe−S linkage from a cysteinate residue.[1,26] Scheme 2 shows the active site of a typical P450 isozyme, namely $P450_{cam}$ (CYP101A1) as taken from the 1DZ9 pdb file.[27] This axial cysteinate ligand exerts a "push" effect on the iron center that has been correlated with the monoxygenase capacity of the enzyme.[28] On the distal side of the heme, the sixth ligand site on the ferric iron is

SCHEME 2: Active Site Structure of the Camphor-Bound Form of $P450_{cam}$[a]

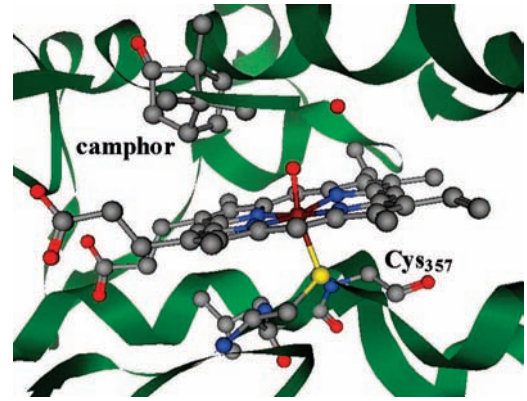

[a] Image was created using MOE and using the atomic coordinates from the 1DZ9 pdb file.

occupied by a water molecule in the resting state. When the substrate enters the active site pocket, this triggers the catalytic cycle that starts with displacement of the water molecule, a shift of the heme iron spin state equilibrium towards high spin, a reduction step, binding of molecular oxygen, a further reduction, and two protonation steps to create an oxo-iron active species.[1] Electrons are delivered via the redox partner iron−sulfur protein putidaredoxin. $P450_{cam}$ regioselectively hydroxylates camphor at the C5 position and has long been used as a model for the structure and function of the P450 class of enzymes. Another structurally and biotechnologically important member of the P450 superfamily is $P450_{BM3}$ (CYP102A1) from *Bacillus megaterium*, in which the P450 is fused to a eukaryotic-like redox partner enzyme—a FAD—and FMN-containing cytochrome P450 reductase (CPR). This makes for a highly efficient electron-transport system, and $P450_{BM3}$ hydroxylates its long-chain fatty acid substrates at rates faster than those of any other known P450 oxidase.[29]

Azole inhibitors occupy the active site space designed for the P450 substrates and bind directly to the heme center, thereby rendering it inactive to oxygen chemistry. There is little available literature on theoretical studies of the binding of azoles to P450 heme. Many azoles contain an imidazole functional group that is expected to bind to the iron center. Imidazole is often used in theoretical studies to model histidine-bound hemes, such as peroxidases, although in those cases, it is located in the proximal axial ligand position occupied by the cysteinate in P450s.[30] In order to gain insight into how azoles bind to P450 enzymes, we have performed a series of density functional theory (DFT) studies. The questions which will be addressed in this work are: why is it that these inhibitors bind so well to the active center and what determines the efficiency of binding? In order to answer these questions, we have performed a series of DFT studies into the mechanisms of azole binding to the heme group of P450 enzymes and have used three typical functional groups representing most azole or azole-like inhibitors.

Methods

All calculations were performed using well-established procedures in the field.[31] We studied the binding of azole models to the active center of cytochrome P450 enzymes. Initial calculations in the gas phase used a minimal model of the resting state of P450 with iron inside of protoporphyrin IX that is ligated to a thiolate axial (proximal) ligand and a water molecule on the distal site. Subsequently, we added an azole mimic and

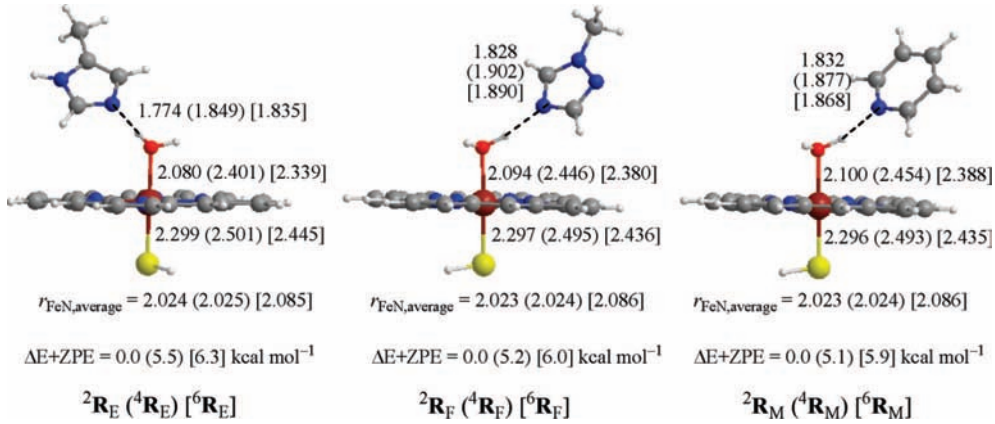

Figure 1. Optimized geometries of $\mathbf{R}_E$, $\mathbf{R}_F$, and $\mathbf{R}_M$ resting state structures in the doublet (quartet) [sextet] spin states. All bond lengths are in Å, and relative energies are in kcal mol^{-1}.

studied the replacement of the water molecule by the azole. Detailed geometry scans with one degree of freedom fixed, namely the distance between the metal and the atom of the azole that binds to iron (Fe−N distance), were performed in Gaussian 03.[32] This procedure, however, did not displace the water molecule from the sixth coordination position of the heme and led to a high-energy pathway. Therefore, an alternative two-dimensional scan was performed where the Fe−OH_2 and Fe−N_{azole} distances were simultaneously scanned. These two-dimensional scans were the result of a full geometry optimization with two degrees of freedom constrained (the Fe−O and Fe−N_{azole} distances).

All calculations described in this work utilize the unrestricted hybrid density functional method UB3LYP (Method M1).[33] Detailed comparative studies on iron porphyrin systems with various density functional methods show that, sometimes, deviations in spin state ordering are observed.[30e] Nevertheless, test calculations (see Supporting Information) using the BP86 functional (Method M2) gave virtually the same results as the ones described in this paper. However, for economy of space, these data are relegated to the Supporting Information.[34] We used a Los Alamos type double-ζ quality basis set that contains a core potential on iron (LANL2DZ), while oxygen and nitrogen are described with 6-31G* and all other atoms with the 6-31G: basis set BS1.[35] Subsequent single-point calculations with a triple-ζ-type LACV3P+ basis set on iron and 6-311+G* on the rest of the atoms (basis set BS2) were performed in Jaguar 7.0.[36] Further test calculations (see Supporting Information) with larger/alternative basis sets showed minimal changes in the binding energies of the various substrates. For all local minima, full optimizations (without constraints) followed by an analytical frequency calculation were performed in Gaussian 03. All local minima described here had real frequencies only, while the transition states were characterized by a single imaginary frequency for the correct mode. The local minima were calculated in the lowest-lying doublet, quartet, and sextet spin states. However, since the doublet spin state was generally the lowest-lying state, we only performed geometry scans for the doublet spin state.

The three inhibitors econazole, fluconazole, and metyrapone were abbreviated to methylimidazolate, methyltriazolate, and pyridine, respectively.

To test the effect of the environment on the azole binding affinities, we tested three different perturbations: (i) by applying a dielectric constant of $\varepsilon = 5.7$ to the system, (ii) with the addition of two hydrogen-bonded ammonia molecules mimicking the peptide environment in the vicinity of the cysteinate ligand, and (iii) a combination of both effects. The calculations with a dielectric constant were performed with the self-consistent reaction field model as implemented in Jaguar 7.0 with a probe radius of 2.7 Å.[36] Previous studies on P450 systems showed that hydrogen bonding toward the cysteinate ligand changes the electronegativity of the sulfur atom and thereby influences the Fe−S bonding interactions strongly.[37] These hydrogen-bonding interactions were shown to be critical for a correct description of the oxo-iron species and were shown to change the regioselectivity of substrate oxidative catalysis.[38] We used the coordinates of the ammonia molecules as described in ref 37 and ran single-point calculations in Jaguar using BS1.

Results

The work described here focuses on the nature of azole binding to the active center of P450 enzymes and how these chemicals work as inhibitors. We studied the binding of three typical azole drugs, each with characteristic features, namely, econazole, fluconazole, and metyrapone. These three inhibitors have different chemical structures that interact with the heme, as shown in Scheme 1 above. Thus, econazole binds the heme with the imidazolate group, which we abbreviated in our model with methylimidazolate. Fluconazole, by contrast, has a characteristic triazolate group that binds the heme, which we abbreviated with methyltriazolate. Finally, metyrapone binds the heme with a pyridine group. The studies started from the resting state of P450, where a water molecule occupies the sixth binding site of iron. Figure 1 shows the optimized geometries of the resting state of P450 (labeled **R**) with an approaching inhibitor molecule. The structures are labeled as based on the inhibitor molecule in the model, with a subscript next to the structure label: E for econazole, F for fluconazole, and M for metyrapone. We calculated all structures in the lowest-lying doublet, quartet, and sextet spin states, as indicated with a superscript. As can be seen from Figure 1, the Fe−S distance is hardly influenced by the nature of the approaching inhibitor but is different for each spin state. This is as expected since in ^{2}**R**, the system has $\delta^2\ \pi^*_{xz}{}^2\ \pi^*_{yz}{}^1$ occupation, while in ^{4}**R** and ^{6}**R**, the orbital occupation is $\delta^2\ \pi^*_{xz}{}^1\ \pi^*_{yz}{}^1\ \sigma^*_{z2}{}^1$ and $\delta^1\ \pi^*_{xz}{}^1\ \pi^*_{yz}{}^1\ \sigma^*_{z2}{}^1\ \sigma^*_{xy}{}^1$, respectively.[28c] Thus, single occupation of the σ^*_{z2} orbital, which is antibonding along the Fe−S bond, will elongate this distance. Relative energies between the doublet, quartet, and sextet spin states are not influenced by the approaching inhibitor molecule either.

The approaching inhibitor molecule forms a hydrogen bond with the water molecule. The Fe−OH_2 distance is influenced

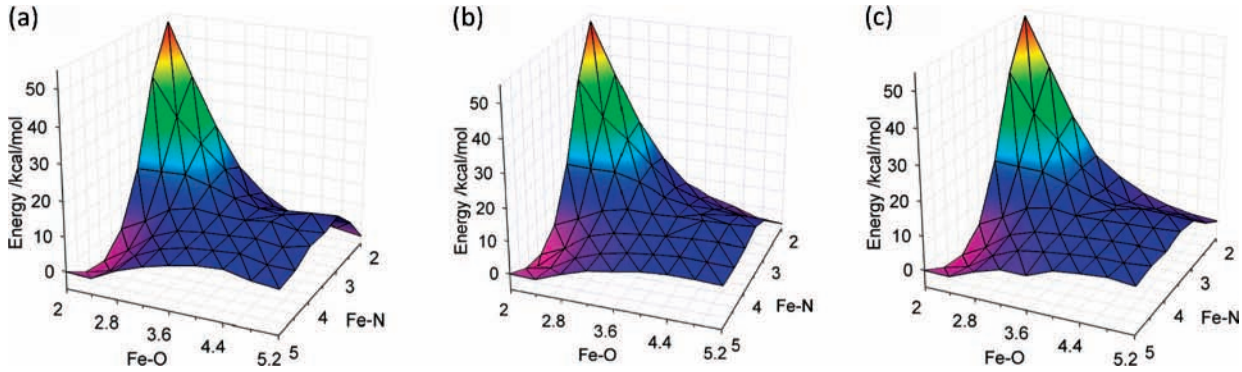

Figure 2. Two-dimensional geometry scans for the simultaneous displacement of water from the active center and for binding of the azole. All data points represent a full geometry optimization in Gaussian 03 with two degrees of freedom fixed (the Fe−OH_2 and Fe−N_{azole} distances) using method M2 and basis set BS1. All energies are in kcal mol^{-1} relative to the resting state. (a) $^2\mathbf{R}_E$ potential energy surface. (b) $^2\mathbf{R}_F$ potential energy surface. (c) $^2\mathbf{R}_M$ potential energy surface.

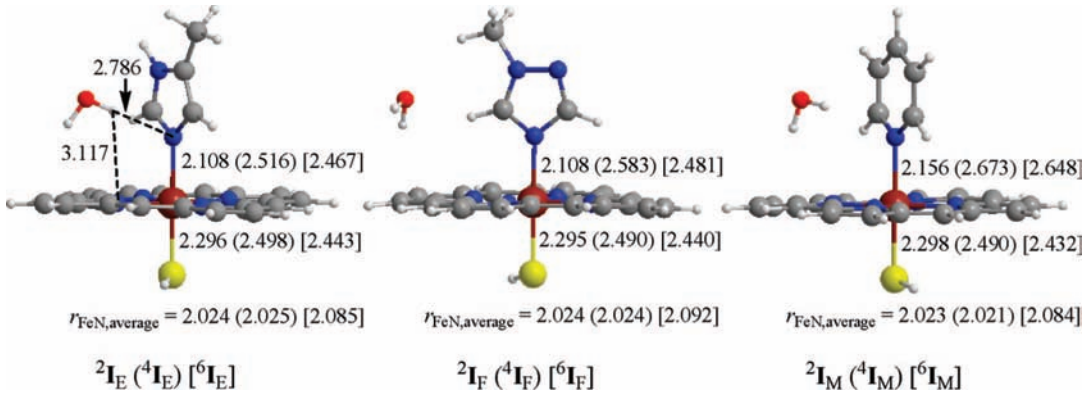

Figure 3. Optimized geometries of $\mathbf{I}_E$, $\mathbf{I}_F$, and $\mathbf{I}_M$ inhibitor complexes in the doublet (quartet) [sextet] spin states. All bond lengths are in Å, and relative energies are in kcal mol^{-1}.

by the strength of the hydrogen bond of the inhibitor molecule and is shortest for $\mathbf{R}_E$ and longest for $\mathbf{R}_M$. The resting state has been extensively studied with experimental as well as theoretical procedures.[30c,39,40] Thus, electron spin-echo envelope modulation (ESEEM) spectroscopy characterized the resting state as a doublet spin state.[39] Detailed quantum mechanical/molecular mechanics (QM/MM) calculations predicted the doublet spin state to be 3.3 and 2.4 kcal mol^{-1} lower in energy than the lowest quartet and sextet states, respectively.[40c] Our calculations shown in Figure 1 support the experimental and theoretical assignments of the resting state from the literature.

To find out how azoles bind to the active center of hemes, we ran extensive geometry scans starting from $^2\mathbf{R}_E$, $^2\mathbf{R}_F$, and $^2\mathbf{R}_M$ for the approach of the azoles to the heme by shortening the Fe−N distance between the heme and the azole. These geometry scans, however, failed to displace the water molecule from the iron center and gave a high-energy pathway. Subsequently, we ran two-dimensional geometry scans for the simultaneous approach of the azole to the heme and the displacement of the water molecule from the heme, and the results are shown in Figure 2. The three inhibitors give the same potential energy surface for the displacement of water by the inhibitor molecule. As follows from these geometry scans, the reaction mechanism is not accomplished with a simultaneous replacement of water by inhibitor. Instead, a stepwise mechanism takes place, with an initial water displacement from the heme site to create a pentacoordinated heme followed by binding of inhibitor to the empty ligand site on the iron. Displacement of water creates a pentacoordinated iron center with a nearby water and inhibitor molecule and with barriers for displacement of the water molecule from $^2\mathbf{R}_E$, $^2\mathbf{R}_F$, and $^2\mathbf{R}_M$ of 15.2, 13.0, and 13.6 kcal mol^{-1}, respectively. These barriers lead to local minima representing a long-range complex between heme, water, and inhibitor and are endothermic by about 13 kcal mol^{-1}. From these long-range complexes, a barrier to the inhibitor-bound complexes (**I**) is crossed. These barriers are 2.3, 1.3. and 0.5 kcal mol^{-1} for econazole, fluconazole, and metyrapone, respectively. As such, the second barrier, that is, for inhibitor binding, is the largest of the two and is likely to be rate-determining. The azole-bound inhibitor complexes are labeled $\mathbf{I}_E$, $\mathbf{I}_F$, and $\mathbf{I}_M$, and their optimized geometries are shown in Figure 3. Binding of inhibitor hardly affects the Fe−S and Fe−N distances in the heme, which are also similar in length. Moreover, these distances are comparable to the ones observed for the resting state complexes (**R**) shown above in Figure 1. The water molecule in the inhibitor-bound complexes ($\mathbf{I}_E$, $\mathbf{I}_F$, and $\mathbf{I}_M$) moves away from the reaction center and out of reach of hydrogen-bonding donors. In most structures, it moves to the meso position of the heme.

The potential energy landscapes shown in Figure 2 seem to imply that inhibitor binding is thermodynamically unfavorable and that the resting state (**R**) is lower in energy than the inhibitor-bound complex (**I**). Of course, this would contradict experiment and would suggest that inhibitors will not be able to displace the water molecule in the resting state. Careful examination of the differences between the structures $\mathbf{R}_E$, $\mathbf{R}_F$, and $\mathbf{R}_M$, on the one hand, and $\mathbf{I}_E$, $\mathbf{I}_F$, and $\mathbf{I}_M$ reveals an extra hydrogen bond in the resting state geometries between the water molecule and the approaching inhibitor, which is missing in the inhibitor-bound complexes. Thus, the loss of the hydrogen bond between the water molecule and the inhibitor that is characteristic for the complexes $\mathbf{R}_E$, $\mathbf{R}_F$, and $\mathbf{R}_M$ artificially

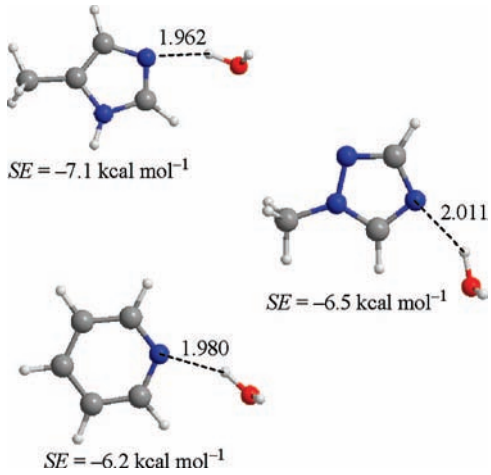

Figure 4. Hydrogen bond energy and hydrogen bond length of methylimidazolate−water, trimethyltriazolate−water, and pyridine−water complexes.

destabilizes the inhibitor-bound complexes in energy. As a result, we find $^2\mathbf{I}_E$, $^2\mathbf{I}_F$, and $^2\mathbf{I}_M$ to be less stable in energy by 3.9, 1.6, and 6.5 kcal mol^{-1} with respect to $^2\mathbf{R}_E$, $^2\mathbf{R}_F$, and $^2\mathbf{R}_M$. This would imply that the inhibitor molecules are less likely to bind the iron active center of P450 enzymes than is a water molecule. However, crystal structures of inhibitor−heme complexes have been clearly resolved, indicating that they are more stable than the resting state (water-bound) structures. Thus, several crystal structures are available with azoles directly bound to the heme iron, that is, in the **I** configuration.[21–23,41]

P450−antifungal azole complexes have been crystallized for Mtb CYP51B1 and CYP121 with fluconazole, for *S. erythraea* $P450_{eryF}$ with ketoconazole, and for rabbit CYP2B4 with bifonazole. Moreover, structures of Mtb CYP51B1 with 4-phenylimidazole, as well as for *P. putida* $P450_{cam}$ with imidazole, have been reported. All show direct coordination of heme iron by a nitrogen atom from the azole drug. On the other hand, the Mtb CYP121 structure with fluconazole revealed two different azole-bound species, one with fluconazole directly bound to the iron and the other with the azole coordinating the heme iron via a bridging water molecule. The indirect binding mode was predominant and was consistent with a constrained CYP121 active site architecture.[23] Thus, these data for CYP121 indicated that alternative binding modes for azole drugs are accessible should steric constraints prevent direct heme iron coordination by the azole.

To estimate the energetic strength of this hydrogen bond between the water molecule and the inhibitor, we ran additional calculations of the inhibitor−water complex and compared the energies with isolated water and inhibitor. The results are shown in Figure 4. In the free inhibitor−water complexes, the hydrogen bond is between 1.962 and 2.011 Å in length, which is significantly longer than that in the resting state complexes in Figure 1, where values between 1.774 and 1.832 Å were found. Therefore, our estimated value of the hydrogen bond strength will be somewhat larger than is actually the case in Figure 1. Thus, the hydrogen bond energies shown in Figure 4 indicate an extra stabilization energy (SE) of the water−inhibitor complexes by at least SE = 6.2−7.1 kcal mol^{-1}. Thus, subtracting the stabilization energy values of the water−inhibitor complexes, as shown in Figure 4 from the reactants complexes, gives a relative energy between the resting state and inhibitor complexes of −3.2 ($\mathbf{I}_E$), −4.9 ($\mathbf{I}_F$), and +0.3 ($\mathbf{I}_M$) kcal mol^{-1}. These corrected relative energies of the inhibitor-bound complexes support experimental findings that the inhibitor-bound complex is more stable than the resting state complexes. However, it appears here that the energy difference is very small; therefore, it may be anticipated that small perturbations within the active pocket may influence the efficiency of inhibitor binding. In the actual enzyme, the broken hydrogen bond between the water molecule and the approaching inhibitor molecule will be replaced by another hydrogen bond to the water inside the active site pocket.

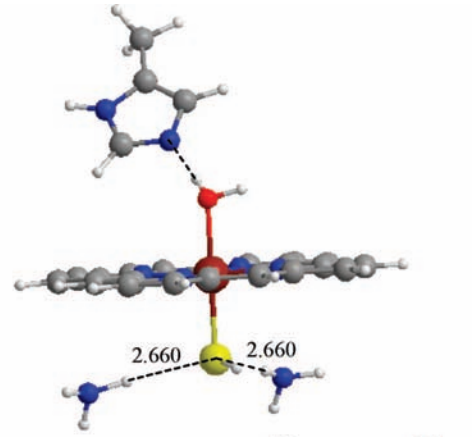

	(*i*) ε = 1 gas-phase, BS2	(*ii*) ε = 1 +2NH$_3$, BS2	(*iii*) ε = 5.7 +2NH$_3$, BS1
$^2\mathbf{R}_E$:	0.0	0.0	0.0
$^2\mathbf{I}_E$:	−6.1	−5.9	−6.7
$^2\mathbf{R}_F$:	0.0	0.0	0.0
$^2\mathbf{I}_F$:	−6.5	−6.5	−5.8
$^2\mathbf{R}_M$:	0.0	0.0	0.0
$^2\mathbf{I}_M$:	−2.0	−1.8	−1.8

Figure 5. The effect of the environment on the ordering of the resting state and azole-bound structures: (i) gas-phase results without external perturbations, (ii) gas-phase model with two extra hydrogen-bonded ammonia molecules, and (iii) system with two hydrogen-bonded ammonia molecules in a dielectric constant of $\varepsilon = 5.7$. All calculations represent single-point energy calculations with either basis set BS1 or BS2. Zero-point energy (ZPE) and stabilization energy (SE) corrections have been included in the data.

Furthermore, the barriers for displacement of the water molecule by the inhibitor molecules from Figure 2 are also overestimated by SE, with values of approximately 6.2−7.1 kcal mol^{-1}. Therefore, the barriers for the displacement of the water molecules from $^2\mathbf{R}_E$, $^2\mathbf{R}_F$, and $^2\mathbf{R}_M$ estimated from the scans in Figure 2 should be lowered by the same amount and are expected instead to be in the range of 8.8, 6.5, and 7.4 kcal mol^{-1}, respectively, for the three processes. Thus, displacement of the water molecule in the resting state of P450 enzymes with an inhibitor molecule will be dependent on the availability of hydrogen-bonding interactions in the active site pocket that can stabilize the leaving water molecule. Moreover, the size and shape of the substrate pocket will determine whether a "perfect fit" of the inhibitor molecule in the pocket is possible.

To find out whether inhibitor binding is influenced by external perturbations, such as solvent polarity or hydrogen bonding, we tested the effect of the local environment on the energy differences of the resting state and azole-bound structures in the doublet spin state. We tested several effects, such as a dielectric constant of value $\varepsilon = 5.7$ and the addition of the hydrogen-bonded ammonia molecules toward the thiolate axial

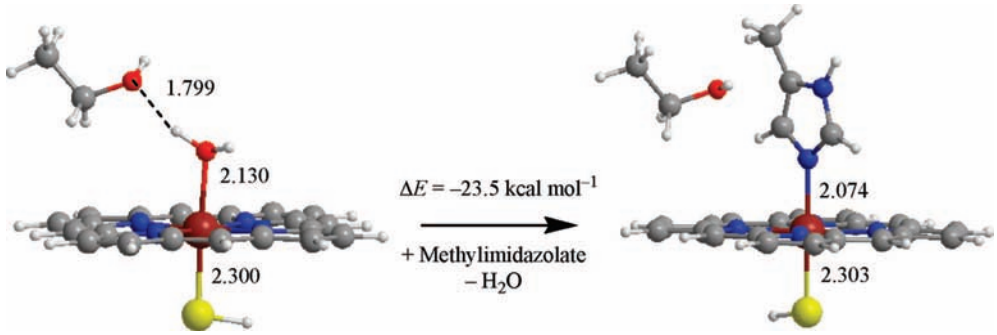

Figure 6. Methylmidazolate-bound P450 structures with a nearby ethanol molecule mimicking Ser_{237} in CYP121. All calculations were performed in Gaussian with a fixed ethanol molecule. Bond lengths shown are in Å.

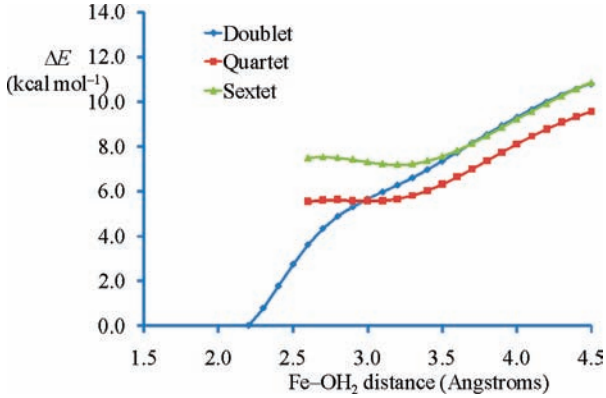

Figure 7. Geometry scans starting from the resting state models (without azole groups) for the dissociation of water from the heme. All data points correspond to a full geometry optimization in Jaguar 7.0 with one degree of freedom (the Fe−O distance) fixed. All energies are in kcal mol^{-1} relative to the optimized geometry of the resting state in the doublet spin state.

ligand; see Figure 5. The latter effect was shown previously to be important for the correct description of the polarity and electronegativity of the iron−sulfur group.[37]

As follows from Figure 5, the azole binding energy is hardly influenced by environmental effects such as a dielectric constant or hydrogen-bonding interactions toward the thiolate group. The calculations do show, however, that pyridine is a much weaker inhibitor than methylimidazolate and methyltriazolate. Therefore, P450 enzymes may not bind pyridine-containing inhibitor molecules strongly. Destabilizing effects of the substrate binding pocket should weaken the inhibitor binding complex by at least 6 kcal mol^{-1} in order to make the two structures comparable in energy. Thus, recent crystallographic evidence showed two alternative inhibitor-bound complexes, one in which the inhibitor is directly bound to the heme (cf. structures **I** above) and one with a water molecule bridging the inhibitor (cf. structures **R** above).[23] The substrate binding pocket of this particular P450 isozyme (CYP121), however, is characterized by a nearby serine (Ser_{237}) amino acid within hydrogen-bonding distance of the heme. To find out how this serine amino acid influences inhibitor binding, we ran calculations with an extra ethanol molecule in our model in the position of Ser_{237} of the CYP121 P450, and the results are shown in Figure 6.

As follows from Figure 6, the resting state structure enjoys a hydrogen bond with the ethanol molecule mimicking Ser_{237}. This, however, does not stabilize the resting state but in fact weakens the Fe−OH_2 bond considerably, which is increased in length from 2.080 Å in $^2\mathbf{R}_E$ to 2.130 Å in Figure 6. As a result of this change, the inhibitor-bound complex is now more stable by 23.5 kcal mol^{-1}. Therefore, hydrogen-bonding interactions within the protein pocket determine the relative stability of the resting state and inhibitor-bound complexes. Moreover, the size and shape of the substrate binding pocket will also clearly determine whether the inhibitor fits easily or not.

Discussion

In this paper, we presented studies on azole inhibition of P450 enzymes. Thus, extensive geometry scans on a resting state model and the approach of azole molecules show that subtle hydrogen-bonding interactions within the active site pocket guide the azole binding process. Azole molecules approach the heme group and are pulled toward it through an accepting hydrogen bond of the resting state water molecule. When the azole molecule approaches the heme closely, the water molecule is released from the heme, and a pentacoordinated heme group remains with nearby azole and water. The azole then replaces the water in the sixth ligand position of the heme, thereby blocking dioxygen binding and rendering the heme centre inactive. The DFT models show that the process is subtle and influenced by hydrogen-bonding donor and acceptor groups within the active site, leading to release of the distal water molecule from the heme iron.

Azole groups bind the heme group and form a covalent linkage with the iron atom with distances of 2.108−2.156 Å in the low-spin states. These distances are similar to those that one would expect for an Fe−N distance in a heme enzyme and have been observed before, for example, for imidazole-ligated iron porphyrin systems mimicking the active site of peroxidases.[30,42] Although, the Fe−N bond between the metal and the azole group is weak, it is of sufficient strength to keep the metal ion in the center (or close to the center) of the porphyrin ring. Thus, previous studies showed that removal of the water molecule from the resting state leads to a displacement of the iron atom well below the porphyrin ring.[28c] As a consequence of this, the orbital mixing patterns are influenced as well. In particular, in strongly distorted systems where the metal is displaced well below the center of the porphyrin ring, the σ^*_{z2} orbital on the metal, representing the antibonding interactions of the metal with the axial cysteinate ligand, mixes with heme-type π^* orbitals, giving the system extra stabilization.[43] Especially in high-spin states where the σ^*_{z2} orbital is singly occupied, this effect is stronger, and, hence, high spin states are stabilized over the low-spin states in pentacoordinated iron porphyrin systems. This means that removal of a water molecule from the resting state should lead to a low-spin to high-spin conversion of the metal center, as indeed observed using, for example, electron paramagnetic resonance (EPR) studies.[44] To find out whether a spin state crossing is expected along the azole binding mechanism, we ran additional geometry scans, but

without the azole molecules removed from the model. In this model, the water molecule is withdrawn from the resting state structure of the heme in small steps. The results are shown in Figure 7 and plotted versus the Fe−O distance for the doublet, quartet, and sextet spin states. As follows from Figure 7, although in the resting state the energy separation between the different spin states is large and well in favor of the doublet spin at Fe−O distances of 2.8 Å or more, the three spin state surfaces approach each other to within 1−2 kcal mol^{-1} at larger distances. In our particular case, the quartet spin state is the ground state of the pentacoordinated complex, and the doublet−quartet spin state crossing appears at around 3.0 Å. Thus, since the azole replacement of the water molecule (Figure 2) leads to a pentacoordinate heme as an intermediate complex, it may very well be that a spin crossing occurs. However, as shown in Figures 2 and 7, no spin crossing is observed in the azole replacement mechanism. Thus, the azole-bound structures are low-spin (doublet) complexes and so are the resting state structures. During the water removal step in the reaction mechanism, the Fe−OH_2 distance is elongated to 3.0−3.5 Å before the azole group moves in. In this region, the quartet and doublet spin states are close in energy, but the system will remain on the doublet since the azole-bound complexes are the lowest in energy on this spin state surface.

Summary and Conclusion

Density functional calculations on inhibitor binding to the active site of P450 enzymes have been studied. It is shown that the relative energies between the resting state and the inhibitor-bound complexes are subtly dependent on small external perturbations. In particular, hydrogen-bonding interactions with either the water molecule in the resting state or with the inhibitor molecule can lead to extra stabilization of one of these states. These factors, together with the "fit" of the inhibitor molecule into the substrate pocket, determine the ordering and the capacity of the azoles to act as an inhibitors.

Acknowledgment. The research was supported by a studentship to P.R.B. from the Medical Research Council (MRC, U.K.) and one to C.S.P. from a Doctoral Training Award (DTA) from the Engineering and Physical Sciences Research Council (EPSRC, U.K.). In addition, research grant funding from the European Union (New Medicines for Tuberculosis, NM4TB) and from the Biotechnology and Biological Sciences Research Council (BBSRC, U.K., Grant Codes BB/F002521/1 and BB/C511305/1) is acknowledged. The Jaguar calculations were done with CPU time provided by the National Service of Computational Chemistry Software (NSCCS).

Supporting Information Available: Cartesian coordinates of all structures described in this work, figures with geometry scans. This material is available free of charge via the Internet at http://pubs.acs.org.

References and Notes

(1) (a) Sono, M.; Roach, M. P.; Coulter, E. D.; Dawson, J. H. *Chem. Rev.* **1996**, *96*, 2841–2887. (b) Ortiz de Montellano, P. R., Ed. *Cytochrome P450: Structure, Mechanism and Biochemistry*, 3rd ed.; Kluwer Academic/Plenum Publishers: New York, 2004. (c) Meunier, B.; de Visser, S. P.; Shaik, S. *Chem. Rev.* **2004**, *104*, 3947–3980. (d) Denisov, I. G.; Makris, T. M.; Sligar, S. G.; Schlichting, I. *Chem. Rev.* **2005**, *105*, 2253–2277. (e) Groves, J. T. *J. Inorg. Biochem.* **2006**, *100*, 434–447.

(2) (a) Guengerich, F. P. *Chem. Res. Toxicol.* **2001**, *14*, 611–650. (b) Ortiz de Montellano, P. R.; De Voss, J. J. Substrate Oxidation by Cytochrome P450 Enzymes. In *Cytochrome P450: Structure, Mechanism, and Biochemistry*, 3rd ed.; Ortiz de Montellano, P. R., Ed.; Kluwer Academic/Plenum Publishers: New York, 2004; Chapter 6, pp 183−245.

(3) Guengerich, F. P. *Drug Metab. Rev.* **2004**, *36*, 159–197.

(4) (a) Guengerich, F. P. *Annu. Rev. Pharmacol. Toxicol.* **1999**, *39*, 1–17. (b) Guengerich, F. P. Human Cytochrome P450 Enzymes. In *Cytochrome P450: Structure, Mechanism, and Biochemistry*, 3rd ed.; Ortiz de Montellano, P. R., Ed.; Kluwer Academic/Plenum Publishers: New York, 2004; Chapter 10, pp 377−530.

(5) Capdevila, J. H.; Falck, J. R.; Imig, J. D. *Kidney Int.* **2007**, *72*, 683–689.

(6) Odds, F. C.; Brown, A. J.; Gow, N. A. *Trends Microbiol.* **2003**, *11*, 272–279.

(7) Feyereisen, R. *Biochem. Soc. Trans.* **2006**, *34*, 1252–1255.

(8) Cole, S. T. *Microbiology* **2002**, *148*, 2919–2928.

(9) McLean, K. J.; Dunford, A. J.; Neeli, R.; Driscoll, M. D.; Munro, A. W. *Arch. Biochem. Biophys.* **2007**, *464*, 228–240.

(10) McLean, K. J.; Warman, A. J.; Seward, H. E.; Marshall, K. R.; Girvan, H. M.; Cheesman, M. R.; Waterman, M. R.; Munro, A. W. *Biochemistry* **2006**, *45*, 8427–8443.

(11) Hollenberg, P. F. *Drug Metab. Rev.* **2002**, *34*, 17–35.

(12) (a) Ferslew, K. E.; Hagardorn, A. N.; Harlan, G. C.; McCormick, W. F. *J. Forensic Sci.* **1998**, *43*, 1082–1085. (b) Kudo, K.; Imamura, T.; Jitsufuchi, N.; Zhang, X. X.; Tokunaga, H.; Nagata, T. *Forensic Sci. Int.* **1997**, *86*, 35–41.

(13) Temple, T. E.; Liddle, G. W. *Annu. Rev. Pharmacol. Toxicol.* **1970**, *10*, 199–218.

(14) Zhang, W.; Ramamoorthy, Y.; Kilicarslan, T.; Nolte, H.; Tyndale, R. F.; Sellers, E. M. *Drug Metab. Dispos.* **2002**, *30*, 314–318.

(15) Ahmad, Z.; Sharma, S.; Khuller, G. K. *FEMS Microbiol. Lett.* **2006**, *262*, 181–186.

(16) Schenkman, J. B.; Remmer, H.; Estabrook, R. W. *Mol. Pharmacol.* **1967**, *3*, 113–123.

(17) Van den Bossche, H. *Curr. Top. Med. Mycol.* **1985**, *1*, 313–351.

(18) Schuster, I. *Xenobiotica* **1985**, *15*, 529–546.

(19) (a) Varhe, A.; Olkkola, K. T.; Neuvonen, P. J. *Clin. Pharmacol. Ther.* **1994**, *56*, 601–607. (b) Park, J. Y.; Shon, J. H.; Kim, K. A.; Jung, H. J.; Shim, J. C.; Yoon, Y. R.; Cha, I. J.; Shin, J. G. *J. Clin. Psychopharmacol.* **2006**, *26*, 135–142. (c) Murayama, N.; Imai, N.; Nakane, T.; Shimizu, M.; Yamazaki, H. *Biochem. Pharmacol.* **2007**, *73*, 2020–2026.

(20) (a) Guardiola-Diaz, H. M.; Foster, L. A.; Mushrush, D.; Vaz, A. D. *Biochem. Pharmacol.* **2001**, *61*, 1463–1470. (b) McLean, K. J.; Cheesman, M. R.; Rivers, S. L.; Richmond, A.; Leys, D.; Chapman, S. K.; Reid, G. A.; Price, N. C.; Kelly, S. M.; Clarkson, J.; Smith, W. E.; Munro, A. W. *J. Inorg. Biochem.* **2002**, *91*, 527–541. (c) Banfi, E.; Scialino, G.; Zampieri, D.; Mamolo, M. G.; Vio, L.; Ferrone, M.; Fermeglia, M.; Paneni, M. S.; Pricl, S. *J. Antimicrob. Chemoth.* **2006**, *58*, 76–84.

(21) (a) Poulos, T. L.; Howard, A. J. *Biochemistry* **1987**, *26*, 8165–8174. (b) Podust, L. M.; Poulos, T. L.; Waterman, M. R. *Proc. Natl. Acad. Sci. U.S.A.* **2001**, *98*, 3068–3073.

(22) (a) Cupp-Vickery, J. R.; Garcia, C.; Hofacre, A.; McGee-Estrada, K. *J. Mol. Biol.* **2001**, *311*, 101–110. (b) Verras, A.; Alian, A.; Ortiz de Montellano, P. R. *Protein Eng., Des. Sel.* **2006**, *19*, 491–496. (c) Ekroos, M.; Sjogren, T. *Proc. Natl. Acad. Sci. U.S.A.* **2006**, *103*, 13682–13687.

(23) Seward, H. E.; Roujeinikova, A.; McLean, K. J.; Munro, A. W.; Leys, D. *J. Biol. Chem.* **2006**, *281*, 39437–39443.

(24) Gorren, A. C. F.; Schmidt, K.; Mayer, B. *Biochemistry* **2002**, *41*, 7819–7829.

(25) (a) Das, A.; Grinkova, Y. V.; Sligar, S. G. *J. Am. Chem. Soc.* **2007**, *129*, 13778–13779. (b) Denisov, I. G.; Grinkova, Y. V.; McLean, M. A.; Sligar, S. G. *J. Biol. Chem.* **2007**, *282*, 26865–26873.

(26) Poulos, T.L.; Raag, R. *FASEB J.* **1992**, *6*, 674–679.

(27) Schlichting, I.; Berendzen, J.; Chu, K.; Stock, A. M.; Maves, S. A.; Benson, D. E.; Sweet, R. M.; Ringe, D.; Petsko, G. A.; Sligar, S. G. *Science* **2000**, *287*, 1615–1622.

(28) (a) Dawson, J. H.; Holm, R. H.; Trudell, J. R.; Barth, G.; Linder, R. E.; Bunnenberg, E.; Djerassi, C.; Tang, S. C. *J. Am. Chem. Soc.* **1976**, *98*, 3707–3709. (b) Poulos, T. L. *J. Biol. Inorg. Chem.* **1996**, *1*, 356–359. (c) Shaik, S.; Kumar, D.; de Visser, S. P.; Altun, A.; Thiel, W. *Chem. Rev.* **2005**, *105*, 2279–2328.

(29) (a) Paine, M. J. I.; Scrutton, N. S.; Munro, A. W.; Gutierez, A.; Roberts, G. C. K.; Wolf, C. R. Electron Transfer Partners of Cytochrome P450. In *Cytochrome P450: Structure, Mechanism, and Biochemistry*, 3rd ed.; Ortiz de Montellano, P. R., Ed.; Kluwer Academic/Plenum Publishers: New York, 2004; Chapter 4, pp 115−148. (b) Warman, A. J.; Roitel, O.; Neeli, R.; Girvan, H. M.; Seward, H. E.; Murray, S. A.; McLean, K. J.; Joyce, M. G.; Toogood, H.; Holt, R. A.; Leys, D.; Scrutton, N. S.; Munro, A. W. *Biochem. Soc. Trans.* **2005**, *33*, 747–753.

(30) (a) Green, M. T. *J. Am. Chem. Soc.* **2000**, *122*, 9495–9499. (b) de Visser, S. P.; Shaik, S.; Sharma, P. K.; Kumar, D.; Thiel, W. *J. Am. Chem. Soc.* **2003**, *125*, 15779–15788. (c) Rydberg, P.; Sigfridsson, E.; Ryde, U. *J. Biol. Inorg. Chem.* **2004**, *9*, 203–223. (d) Derat, E.; Shaik, S. *J. Am. Chem. Soc.* **2006**, *128*, 8185–8198. (e) Groenhof, A. E.; Swart, M.; Ehlers, A. W.; Lammertsma, K. *J. Phys. Chem. A* **2005**, *109*, 3411–3417.

(31) (a) de Visser, S. P. *J. Am. Chem. Soc.* **2006**, *128*, 9813–9824. (b) de Visser, S. P. *J. Am. Chem. Soc.* **2006**, *128*, 15809–15818. (c) Aluri, S.; de Visser, S. P. *J. Am. Chem. Soc.* **2007**, *129*, 14846–14847.

(32) Frisch, M. J. Trucks, G. W.; Schlegel, H. B.; Scuseria, G. E.; Robb, M. A.; Cheeseman, J. R.; Montgomery, J. A., Jr.; Vreven, T.; Kudin, K. N.; Burant, J. C.; Millam, J. M.; Iyengar, S. S.; Tomasi, J.; Barone, V.; Mennucci, B.; Cossi, M.; Scalmani, G.; Rega, N.; Petersson, G. A.; Nakatsuji, H.; Hada, M.; Ehara, M.; Toyota, K.; Fukuda, R.; Hasegawa, J.; Ishida, M.; Nakajima, T.; Honda, Y.; Kitao, O.; Nakai, H.; Klene, M.; Li, X.; Knox, J. E.; Hratchian, H. P.; Cross, J. B.; Bakken, V.; Adamo, C.; Jaramillo, J.; Gomperts, R.; Stratmann, R. E.; Yazyev, O.; Austin, A. J.; Cammi, R.; Pomelli, C.; Ochterski, J. W.; Ayala, P. Y.; Morokuma, K.; Voth, G. A.; Salvador, P.; Dannenberg, J. J.; Zakrzewski, V. G.; Dapprich, S.; Daniels, A. D.; Strain, M. C.; Farkas, O.; Malick, D. K.; Rabuck, A. D.; Raghavachari, K.; Foresman, J. B.; Ortiz, J. V.; Cui, Q.; Baboul, A. G.; Clifford, S.; Cioslowski, J.; Stefanov, B. B.; Liu, G.; Liashenko, A.; Piskorz, P.; Komaromi, I.; Martin, R. L.; Fox, D. J.; Keith, T.; Al-Laham, M. A.; Peng, C. Y.; Nanayakkara, A.; Challacombe, M.; Gill, P. M. W.; Johnson, B.; Chen, W.; Wong, M. W.; Gonzalez, C.; Pople, J. A. *Gaussian 03*, Revision C.02; Gaussian, Inc.: Wallingford, CT, 2003.

(33) (a) Becke, A. D. *J. Chem. Phys.* **1993**, *98*, 5648–5652. (b) Lee, C.; Yang, W.; Parr, R. G. *Phys. Rev. B* **1988**, *37*, 785–789.

(34) (a) Becke, A. D. *Phys. Rev. A* **1988**, *38*, 3098–3100. (b) Perdew, J. P. *Phys. Rev. B* **1986**, *33*, 8822–8824.

(35) Hay, P. J.; Wadt, W. R. *J. Chem. Phys.* **1985**, *82*, 270–283.

(36) *Jaguar 7.0*; Schrödinger, LLC.: New York, NY, 2007.

(37) Ogliaro, F.; Cohen, S.; de Visser, S. P.; Shaik, S. *J. Am. Chem. Soc.* **2000**, *122*, 12892–12893.

(38) (a) de Visser, S. P.; Ogliaro, F.; Sharma, P. K.; Shaik, S. *Angew. Chem., Int. Ed* **2002**, *41*, 1947–1951. (b) de Visser, S. P.; Ogliaro, F.; Sharma, P. K.; Shaik, S. *J. Am. Chem. Soc.* **2002**, *124*, 11809–11826. (c) de Visser, S. P.; Shaik, S. *J. Am. Chem. Soc.* **2003**, *125*, 7413–7424. (d) de Visser, S. P. *Chem.—Eur. J.* **2006**, *12*, 8168–8177.

(39) Thomann, H.; Bernardo, M.; Goldfarb, D.; Kroneck, P. M. H.; Ullrich, V. *J. Am. Chem. Soc.* **1995**, *117*, 8243–8251.

(40) (a) Green, M. T. *J. Am. Chem. Soc.* **1998**, *120*, 10772–10773. (b) Filatov, M.; Harris, N.; Shaik, S. *J. Chem. Soc., Perkin Trans. 2* **1999**, *3*, 399–411. (c) Schöneboom, J. C.; Thiel, W. *J. Phys. Chem. B* **2004**, *108*, 7468–7478.

(41) Zhao, Y. H.; White, M. A.; Muralidhara, B. K.; Sun, L.; Halpert, J. R.; Stout, C. D. *J. Biol. Chem.* **2006**, *281*, 5973–5981.

(42) de Visser, S. P. *J. Phys. Chem. A* **2005**, *109*, 11050–11057.

(43) de Visser, S. P.; Ogliaro, F.; Gross, Z.; Shaik, S. *Chem.—Eur. J.* **2001**, *7*, 4954–4960.

(44) (a) Sligar, S. G. *Biochemistry* **1976**, *15*, 5399–5406. (b) Auclair, K.; Moënne-Loccoz, P.; Ortiz de Montellano, P. R. *J. Am. Chem. Soc.* **2001**, *123*, 4877–4885.

JP802087W